

# Dust Attenuation in Hydrodynamic Simulations of Spiral Galaxies

Miguel Rocha,<sup>1\*</sup> Patrik Jonsson,<sup>1†</sup> Joel R. Primack,<sup>1,2‡</sup> and T.J. Cox<sup>3§</sup>

<sup>1</sup>*Santa Cruz Institute for Particle Physics, University of California, Santa Cruz, CA 95064*

<sup>2</sup>*Department of Physics, University of California, Santa Cruz, CA 95064*

<sup>3</sup>*Harvard-Smithsonian Center for Astrophysics, Cambridge, MA 02138*

4 August 2021

## ABSTRACT

We study the effects of dust in hydrodynamic simulations of spiral galaxies when different radial metallicity gradients are assumed. SUNRISE, a Monte-Carlo radiative-transfer code, is used to make detailed calculations of the internal extinction of disk galaxies caused by their dust content.

SUNRISE is used on eight different Smooth Particle Hydrodynamics (SPH) simulations of isolated spiral galaxies. These galaxies vary mainly in mass and hence luminosity, spanning a range in luminosities from  $-16$  to  $-22$  magnitudes in the B band. We focus on the attenuation in different wavelength bands as a function of the disk inclination and the luminosity of the models, and compare this to observations.

Observations suggest different metallicity gradients for galaxies of different luminosities. These metallicity gradients were explored in our different models, finding that the resulting dust attenuation matches observations for edge-on galaxies, but do not show a linear behaviour in log axis ratio as some observations have suggested. A quadratic law describing the dependence of attenuation on inclination, as proposed by more recent observations, reconciles the attenuation of the simulations at intermediate inclinations with observations. We also compare the total infrared-to-ultraviolet flux ratios for the simulated galaxies with those of the SINGS sample and find general agreement. Finally we compare our results with those from simpler models that do not take into account structure such as spiral arms, finding that the inclusion of sub-structure on the size scale of spiral arms does not change conclusions about the attenuation dependence on inclination or wavelength.

**Key words:** dust — radiative transfer — galaxies: spiral — methods: numerical

## 1 INTRODUCTION

Studies of dust extinction in spiral galaxies play an important role in this time of precision cosmology. It is remarkable how, despite the fact that distances have always been one of the most challenging measurements in astronomy, we are now able to obtain accurate cosmological distances to galaxies and galaxy clusters. This is possible because of relations like the Tully-Fisher relation (hereafter TF) and the Fundamental Plane, which relate observable parameters of galaxies, such as  $H_I$  velocity profile widths and central velocity dispersions, to their luminosity and radius. Given that these methods are independent of redshift, they are also important in determining the Hubble constant (Freedman et al. 2001) and peculiar velocities of galaxies (i.e., the difference between Hubble velocities and redshift velocities). With this, one can also obtain a potential (Bertschinger et al. 1990) that can be used to compare the ob-

served galaxy distributions and kinematics to cosmological predictions (e.g. Dekel et al. 1999). Nevertheless, these valuable relations are subject to extinction corrections that are important to take into account. The scatter in the TF relation is increased if the extinction correction that depends on the disk inclination is not well understood. Even more so, the slope of the TF relation may be affected by corrections for the luminosity dependence of extinction. The dependencies of the TF relation on such corrections are demonstrated in detail in Giovanelli et al. (1995, hereafter G95).

Furthermore, hierarchical models of galaxy formation predict that the disks of spiral galaxies form from the inside out, having younger stellar populations and lower metallicity in the outer disk. Thus, quantifying the gradients in the metallicity distribution of galaxies with different luminosities is important in order to compare the predictions of hierarchical models with observations. This can be done by looking at the effects that different metallicity gradients have on the attenuation of disk galaxies, and comparing the results with observations.

Another motivation for studying the attenuation of dust in the disk of spiral galaxies is to gain insight into how the dust is distributed. The attenuation vs. inclination relations of a galaxy

\* E-mail: mrocha@scipp.ucsc.edu

† E-mail: patrik@ucolick.org

‡ E-mail: joel@scipp.ucsc.edu

§ E-mail: tcox@cfa.harvard.edu

completely free of dust and a completely opaque galaxy in which the obscuring dust is confined to a thin layer in the mid-plane of the disk are difficult to distinguish, except when seen close to edge-on. This is one of the reasons why determining the degree of dust attenuation in a galaxy is difficult, and has led to a long-standing debate about the extent to which galaxy disks are transparent or opaque (Disney et al. 1989; Burstein et al. 1991; Bosma et al. 1992; Disney et al. 1992; Valentijn 1994; Kylafis et al. 2001; Holwerda et al. 2005). Further studies (Moriondo et al. 1998; Xilouris et al. 1999) indicate that central regions of the disk may be opaque while outer regions are transparent. Observations reveal that the surface intensity in spirals falls off exponentially with radius (de Vaucouleurs 1948) while in the vertical direction both the stars (van der Kruit & Searle 1981) and the gas and dust (Cowie & Songaila 1986; Kylafis & Bahcall 1987) fall off roughly exponentially with height. Exponential models of galaxies with equal dust and stellar scalelengths have previously been used to study dust attenuation (Disney et al. 1989). Xilouris et al. (1999, hereafter X99) fit exponential models to observations of seven spiral galaxies seen very close to edge-on (NGC 4013, IC 2531, UGC 1082, NGC 5529, NGC 5907, UGC 2048, and NGC 891), and revealed that in general these large spirals possess a dust scalelength that is about 1.4 times larger than that of the stars, and a vertical dust scaleheight that is about half that of the stars. These data indirectly suggest a metallicity gradient that will have different effects on the shape and amplitude of the attenuation vs. inclination relation. Consequently, exploring this relation can lead to conclusions about the radial distribution properties of the dust in the disk of spiral galaxies.

Other observations have quantified the metallicity gradient of spiral galaxies by different methods. Zaritsky et al. (1994, hereafter Z94) provides the metallicity gradient of 39 disk galaxies, by examining the properties of HII regions within the disk of these galaxies. They found an average metallicity gradient of  $-0.05$  dex/kpc, although this value varied widely from 0.00 to  $-0.20$  dex/kpc. They found a correlation between abundance gradients and Hubble type only when the gradients are expressed in terms of dex/kpc as opposed to dex/isophotal radius.

Based on the fact that colour gradients in disk galaxies are due in most part to the gradients in age and metallicity (Bell & de Jong 2000), MacArthur et al. (2004, hereafter MA04) provided results of metallicity gradients from observations of optical and NIR galaxy colour gradients in a sample of 172 galaxies with different luminosities. They found that the metallicity gradients in their sample were steeper than those of Z94 for galaxies fainter than  $\sim -20$ , and shallower for galaxies brighter than  $\sim -20$ , in the K-band.

G95 sampled more than 1700 galaxies for which I-band CCD images, redshifts, and HI line widths were available. Their conclusions were that their attenuation as a function of inclination could be well fitted by a linear function of  $\log(a/b)$ , where  $a/b$  is the axis ratio. From sampling 87 spiral galaxies within the Ursa Major and Pisces Clusters, Tully et al. (1998, hereafter T98) reached conclusions similar to those of G95, with their data fitting well a linear relation. Masters et al. (2003, hereafter M03) based their results on data taken from 3035 galaxies from the 2 Micron All-Sky Survey (2MASS Jarrett et al. 2001, 2003) for which I-band photometry and redshifts were available, and concluded that a simple linear law was not adequate for describing the attenuation dependence on inclination observed in their sample. Thus, M03 adopted a bilinear law fitting separately high and low inclinations systems as separated by  $\log(a/b) = 0.5$ . Looking for even less linear shapes that fit their observed colour dependence on inclination, M03 also

tried a quadratic law. The results provided by M03 and G95 cover only the infrared and near infrared range of the spectrum.

Here we use the capabilities of SUNRISE, a Monte Carlo radiative-transfer code (Jonsson 2006), to perform “simulated observations” of dust attenuation in the disks of eight different hydrodynamic simulations of spiral galaxies, having different luminosities and sizes, while assuming the different metallicity gradients provided by MA04, X99, and Z94. Performing these “simulated observations” at different inclinations for each of the galaxy models, we obtain the attenuation dependencies on inclination and luminosity for each of the assumed metallicity distributions. These results are then compared to the observations made by M03, G95, and T98. By finding which simulations best fit the data, it is determined which metallicity gradients are the most appropriate for these galaxy models.

The main difference between this work and previous ways of quantifying the attenuation produced by dust in galaxies through radiative transfer calculations is that our calculations are performed over an arbitrary geometry specified by the hydrodynamic simulations. Thus our galactic models resolve structure such as spiral arms that in previous radiative transfer models, either by analytical approximations (Byun et al. 1994; Silva et al. 1998; Xilouris et al. 1999; Baes & Dejonghe 2001; Tuffs et al. 2004) or by Monte Carlo calculations (de Jong 1996; Kuchinski et al. 1998; Ferrara et al. 1999; Bianchi et al. 1996, 2000; Matthews & Wood 2001; Pierini et al. 2004), is not considered. Nevertheless, the structure resolved in our simulations is not small enough to include individual star forming regions, which affects the resulting attenuation. We compare our results with previous models to examine if the inclusion of structures such as spiral arms makes a difference in the dependence of attenuation on inclination and wavelength. Finally we have extended the triple exponential model of Disney et al. (1989) to explore how the dependence of attenuation on inclination changes with different dust-to-star scalelengths ratios.

The structure of this paper is as follows: Section 2 is a presentation of the hydrodynamic galaxy models. In section 3, a description is given of how the simulated observations were made with SUNRISE. In section 4 the results are compared to real observations. In section 5 we compare to previous models of galactic disks without structure such as spiral arms, and explore how the dependence of attenuation on inclination changes with different dust-to-star scalelength ratios. Section 6 provides a summary and lists the conclusions.

## 2 THE HYDRODYNAMIC GALAXY MODELS

Radiative-transfer calculations were made for eight different Smooth Particle Hydrodynamics (SPH) simulations of isolated galaxies. These simulated galaxies were created using a version of the code GADGET1 which enables entropy conservation (Springel et al. 2001; Springel & Hernquist 2002), as part of a comprehensive work aimed at studying galaxy mergers (Cox 2004; Cox et al. 2006, 2007; Jonsson et al. 2006; Jonsson 2006).

The set of isolated galaxies for which calculations of dust extinction were made includes four models that approximate late-type spiral galaxies and four less gas-rich spiral galaxies (the G-series). The late-type spirals group comprises an Sbc type galaxy, a more massive and bigger Sbc (Sbc+), a less massive and smaller Sbc (Sbc-), and an Sc type. The G-series have been created spanning a wide range of masses and having average properties for their mass. Table 1 lists the characteristic of each model. The details of these

galaxy models are described in Cox et al. (2006) and Jonsson et al. (2006). Here we mention some of their important features.

The galaxies contain a stellar and gaseous disk, which are rotationally supported, a spheroidal stellar bulge, and a massive dark matter halo. A model for supernova feedback, as described in Cox et al. (2006), is included and is crucial for the stability of the gas disk and for preventing excessive star formation. The adopted star formation prescription is based on a Schmidt law (Schmidt 1959) and is consistent with the Kennicutt law (Kennicutt 1998). Schemes for radiative cooling and metal enrichment have also been implemented in these models. Our models do lack age gradients, something that would be necessary for comparing our results with the predictions of hierarchical models of galaxy formation.

### 3 THE RADIATIVE TRANSFER CALCULATIONS

#### 3.1 SUNRISE

SUNRISE is a high-performance code designed to combine a full radiative-transfer model with high-resolution hydrodynamic simulations of either isolated or interacting galaxies; see Jonsson (2006) for a detailed description of how SUNRISE achieves this goal. SUNRISE first assigns an initial spectral energy distribution (SED) for the stellar particles in the hydrodynamic simulations. Assuming that the density of dust traces the density of metals, it then solves the radiative-transfer problem by the Monte-Carlo method in the given arbitrary geometry for a number of wavelengths, and finally, it interpolates to obtain a resulting full SED after absorption and scattering. The SEDs used are from Starburst99<sup>1</sup> v5.0 (Leitherer et al. 1999) with Kroupa IMF. In post-processing, SUNRISE calculates total magnitudes and generates images for the specified optical filter bands, as well as the total absorbed bolometric luminosity, over all wavelengths. In this way SUNRISE can be used to make simulated observations that can be easily compared to actual observations. SUNRISE is free software<sup>2</sup>.

For this investigation, calculations have been done using eight different filters (U, B, V, R, I, J, H and K) and thirteen cameras at different inclinations. Six cameras were placed above the plane of the disk at inclination angles 0, 35, 51, 63, 74, and 85 degrees. Another six were placed at the same inclinations but on the opposite side of the disk and at a 90 degree azimuthal angle to the first set. One more camera was placed exactly edge-on. These calculations were done for two simulation times, 0.5 Gyr and 1 Gyr. This allows enough time for the simulation to relax but is not so late that a significant amount of gas is consumed. For each inclination, the results were averaged over the two azimuthal angles and the two snapshots. For simplicity, the dust model used in all our models regardless of size was the  $R = 3.1$  Milky-Way model by Weingartner & Draine (2001).

#### 3.2 Star-Formation History and Metallicity Distributions

Given that the metallicity and the age are required to pick the SED of a stellar particle, two important values that are given as inputs to SUNRISE are the star-formation history and the metallicity distribution of the stars present when the simulation is started.

In all the calculations made for this paper the bulge stars are assumed to have formed in an instantaneous burst, while the disk

has had an exponentially declining star-formation rate starting at the time of bulge formation and leading up to the start of the simulation. The age of the bulge and stars at the beginning of the simulation, and the time constant  $\tau$  of the exponential decline used for each of the galaxy models are given in Table 1. The time constant  $\tau$  for each galaxy was determined by fitting an exponential star formation rate history to the following constraints: the present-day star-formation rate must match the star formation rate in the hydrodynamic simulations, the total stellar mass must match that in the simulated models, the average stellar age must match the data in MA04 (as well as possible), and finally no stars can be older than a Hubble time. In the case of the Sc galaxy, this means a marginally growing star-formation rate (at the onset of star formation 13.8 Gyr ago, the star formation rate was 37% of the present-day SFR). This is not very surprising, since a large, gas rich spiral today cannot have sustained its large star formation rate for a long time without exceeding its current stellar mass, it's just being assembled later than average. Effectively, the very large numbers (positive as well as negative) just mean a constant star formation rate history.

The metallicity of the gas and stars at the start of the simulation is, like the surface densities, assumed to decline exponentially with radius in the disk. The metallicity of the gas particles is assumed to be the same as that of the stars and thus the same dependence applies for the gas metallicity as a function of radius. Dwek (1998) concluded that the formation of dust grains in the interstellar medium is, in good approximation, linearly proportional to the density of metals, with a proportionality constant of 0.4. If that is the case, the dust density  $d(r)$  would also decline exponentially from the centre as is observed by X99, and be described by a relation of the form

$$d(r) = 0.4g(r)z(r) = d_o e^{-r/R_g} 10^{-Gr} = d_o e^{-r/R_d}, \quad (1)$$

with  $R_g$  and  $R_d$  being the gas and dust scalelengths respectively,  $d_o = 0.4z_o g_o$  being the central density of dust, and  $G$  being a constant that determines the gradient of a metallicity distribution expressed in a decimal exponential manner, as is usually given (Z94, MA04). The observations of X99, as described in Section 1, suggest that the dust scalelength of big spiral galaxies is about 1.4 times greater than the stellar scalelength. Hence, we can define the ‘‘Xilouris gradient’’  $G_X$  as the gradient that results in a ratio of dust scalelength to stellar scalelength equal to 1.4. Recalling equation 1 we have that

$$e^{-r/R_g} 10^{-G_X r} = e^{-r/R_d} = e^{-r/1.4R_s}, \quad (2)$$

or

$$G_X = \left( \frac{1}{1.4R_s} - \frac{1}{R_g} \right) \log e. \quad (3)$$

The Xilouris gradient  $G_X$  for each of the galaxy models is shown in Table 2.

X99 observed only big spiral galaxies, so  $G_X$  is not necessarily the best metallicity gradient assumption for our set of smaller galaxies. MA04 (Fig. 26) provides metallicity gradients as a function of luminosity for a sample of 127 galaxies, from which we have obtained another set of gradients that were applied to the three smallest galaxies, G2, G1 and G0. Table 2 shows these last gradients and summarises all the gradients that were tested in the simulations.

It is important to note that the central metallicity of the galaxies depends on the gradient in use. This is because the metallicity given in Table 1 is at 1.3 scalelengths from the centre.

<sup>1</sup> <http://www.stsci.edu/science/starburst99/>

<sup>2</sup> <http://sunrise.familjenjonsson.org>

**Table 1.** The galaxy models used for the calculations of dust attenuation.

Model	$M_{\text{vir}}^{\text{a}}$ ( $M_{\odot}$ )	$M_b^{\text{b}}$ ( $M_{\odot}$ )	$R_d^{\text{c}}$ (kpc)	$Z_d/R_d^{\text{d}}$	$R_g/R_d^{\text{e}}$	$f_g^{\text{f}}$	$f_b^{\text{g}}$	$R_b^{\text{h}}$ (kpc)	$V_{\text{rot}}^{\text{i}}$ km/s	$Z_{1.3}^{\text{j}}$ ( $Z_{\odot}$ )	$N_g^{\text{k}}$ ( $\times 10^4$ )	Age <sup>l</sup> (Gyr)	$\tau^{\text{m}}$ (Gyr)
Sbc+	$9.28 \cdot 10^{11}$	$1.56 \cdot 10^{11}$	7.0	0.125	3.0	0.52	0.10	0.60	210	1.12	3	13.9	110
Sc	$8.90 \cdot 10^{11}$	$1.12 \cdot 10^{11}$	4.7	0.2	4.0	0.69	0.00	0.00	196	1.00	3	13.8	-13
Sbc	$8.12 \cdot 10^{11}$	$1.03 \cdot 10^{11}$	5.5	0.125	3.0	0.52	0.10	0.45	195	1.00	3	13.9	-106
G3	$1.16 \cdot 10^{12}$	$6.22 \cdot 10^{10}$	2.8	0.125	3.0	0.20	0.14	0.37	192	1.00	5	14.0	10
Sbc-	$3.60 \cdot 10^{11}$	$4.98 \cdot 10^{10}$	4.0	0.125	3.0	0.52	0.10	0.40	155	0.70	3	13.7	124
G2	$5.10 \cdot 10^{11}$	$1.98 \cdot 10^{10}$	1.9	0.2	3.0	0.23	0.08	0.26	139	0.56	3	14.0	8.2
G1	$2.00 \cdot 10^{11}$	$7.00 \cdot 10^9$	1.5	0.2	3.0	0.29	0.04	0.20	103	0.40	2	11.5	3.7
G0	$5.10 \cdot 10^{10}$	$1.60 \cdot 10^9$	1.1	0.2	3.0	0.38	0.01	0.15	67	0.28	1	8.7	1.4

<sup>a</sup>Virial mass.<sup>b</sup>Baryonic mass.<sup>c</sup>Stellar disk scalelength.<sup>d</sup>Ratio of stellar-disk scaleheight and scalelength.<sup>e</sup>Ratio of scalelengths of gas and stellar disks.<sup>f</sup>Gas fraction (of baryonic mass).<sup>g</sup>Bulge fraction (of baryonic mass).<sup>h</sup>Bulge scale radius.<sup>i</sup>Circular velocity.<sup>j</sup>Metallicity at 1.3 scalelengths from the centre (gas and stars), from Z94.<sup>k</sup>Number of gas particles.<sup>l</sup>Age of oldest stars (formation time of bulge and oldest disk stars).<sup>m</sup>Exponential time constant of the star formation rate for the disk stars.**Table 2.** Tested Metallicity Gradients.

Galaxy	Z94 ( $-dex \text{ kpc}^{-1}$ )	X99 ( $G_X$ ) ( $-dex \text{ kpc}^{-1}$ )	MA04 ( $-dex \text{ kpc}^{-1}$ )
Sbc+	0.05	<b>0.023</b>	-
Sc	0.05	<b>0.043</b>	-
Sbc	0.05	<b>0.030</b>	-
G3	0.05	<b>0.058</b>	-
Sbc-	0.05	<b>0.041</b>	-
G2	0.05	0.086	<b>0.04</b>
G1	0.05	0.112	<b>0.05</b>
G0	0.05	0.148	<b>0.06</b>

The adopted metallicity gradients in our models are shown in bold.

The advantage of producing simulated observations with SUNRISE is that the results of the calculations can be directly compared to observations, which will be done in the next section.

## 4 RESULTS AND COMPARISON WITH OBSERVATIONS

Before analysing any data, we can anticipate some of the results by simply looking at the colour composite images obtained in our calculations. Figure 1 clearly shows the effects of having or not having a metallicity gradient when the Sbc model is seen edge-on, while Figure 2 shows how the metallicity, and hence the strength of the dust lane and attenuation, decrease with luminosity. Note that Dalcanton et al. (2004) found that galaxies with rapidly rotating disks (i.e.  $V_{\text{rot}} > 120$  km/s) have well defined dust lanes, while galaxies with lower rotation velocities do not show evident dust lanes. Figure 2 shows that it is hard to see any dust lanes in our G2 and smaller galaxy models, which have rotation velocities of less than 139 km/s (See Table 1).

### 4.1 Observations of Disk Attenuation.

Some of the results of G95, T98, and M03 will be used to compare the data obtained from our simulations with observations. These authors have quantified the extinction effects in the disks of galaxies as a function of inclination, with an aim to better understand the necessary extinction corrections to the TF relation. The extinction effects of dust are normally quantified by measuring the attenuation, which refers to the decrease in flux resulting from photons being scattered and/or absorbed. This is defined as

$$A_{\lambda} = m_{\lambda}^0 - m_{\lambda} = -2.5 \log \left( \frac{f_{\lambda}^0}{f_{\lambda}} \right), \quad (4)$$

with  $m_{\lambda}^0$  and  $f_{\lambda}^0$  being the intrinsic magnitude and flux in the absence of dust respectively. In the simulations, it is simple to find the attenuation dependence on inclination of a galaxy by simply computing the attenuation, as in equation 4, for a number of different lines of sights at different inclinations. In real systems, it is not easy to determine the actual inclination of the disk and it is impossible to know the intrinsic magnitude or flux by direct measurement, hence more practical ways of defining inclination and attenuation are required.

The technique used (G95, T98 and M03) to find the inclination is by first determining an isophotal radius (a radius of constant surface brightness) in the disk of the observed galaxies, and then finding the ratio between the semi-major and the semi-minor axis of the isophotal ellipse, which is related to the actual inclination by

$$\cos i = \sqrt{\frac{(b/a)^2 - q^2}{1 - q^2}}, \quad (5)$$

where  $a$  and  $b$  are the semi-major and semi-minor axis respectively, and  $q$  is the axial ratio when the system is viewed edge-on. Having this and given that surface brightness is proportional to the flux, one could expect that, as a simple approximation, the attenuation relative to face-on as a function of axial ratio would follow a relation



**Figure 1.** Colour composite images (I,V,B bands) of the Sbc model with no dust, assuming the Xilouris gradient, and assuming constant metallicity for top, middle, and bottom respectively. We can see a significant difference between these three cases when edge-on.

of the form

$$A_\lambda = \gamma_\lambda \log \left( \frac{\text{face-on area} = \pi a^2}{\text{inclined area} = \pi ab} \right) = \gamma_\lambda \log \left( \frac{a}{b} \right), \quad (6)$$

where  $\gamma_\lambda$  is an attenuation parameter as a function of wavelength  $\lambda$  and luminosity. Of course this would be completely valid only if the surface brightness of the system were constant. G95, T98 and M03 fitted their observations with a relation of the form of equation 6 and with that obtained the most appropriate value of  $\gamma_\lambda$ .

Since it is not possible to know the intrinsic magnitudes and these observers were only interested in the dependence on inclination of the attenuation in a given band, the observations used for their fits were those of the  $\lambda - K$  colour (where  $\lambda$  can be any given band). This is because dust is optically thin in the near infrared part of the spectrum, and thus the magnitude in K should be approximately constant with inclination. Thus, the main technique used for these observations is to find the  $\gamma_\lambda$  that best fits their observations of the dependence of the colour  $\lambda - K$  on the axial ratio  $a/b$ . Under the assumption that extinction effects in the K-band are negligible and independent of inclination, the dependence of  $\lambda - K$  colour on inclination would then represent the actual attenuation dependence on inclination for the given band  $\lambda$ .

T98 assumed that the extinction effects in the K-band, although small, were not entirely negligible. They concluded that their results of attenuation as a function of inclination were well fit by a linear relation in logarithmic space that followed the form of equation 6 (see Fig 2 in T98), with a slope  $\gamma_\lambda$  that is dependent on luminosity. Their adopted equations for  $\gamma_B$  and  $\gamma_I$  were

$$\gamma_B = -0.35(15.6 + M_B + 5 \log h_{80}) \quad (7)$$

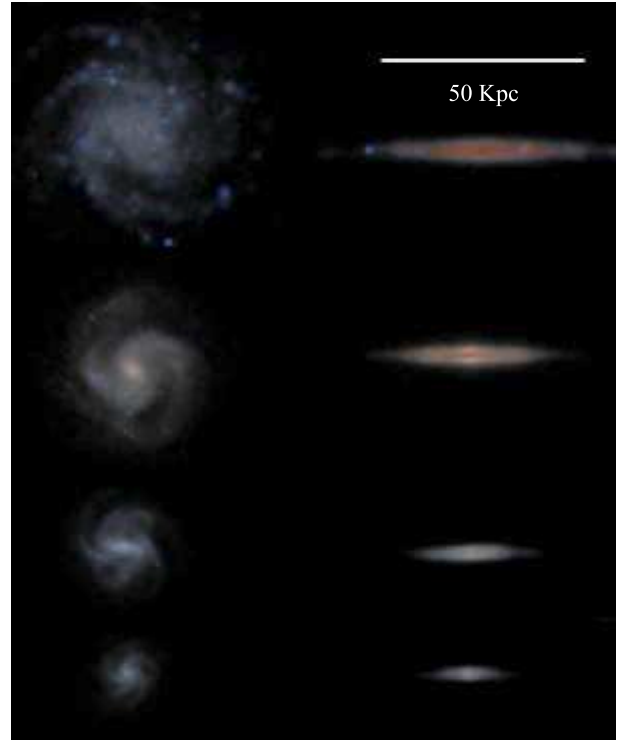


**Figure 2.** Face-on and edge-on colour composite images (I,V,B bands) of the Sc, G3, G2 and G1 galaxy models from top to bottom respectively. The scale is the same so that the differences in size can be visualised. The G0, which is not shown here, is even smaller and less luminous than the G1 (see Table 1). Notice how the strength of the dust lane and the reddening decreases with the size (luminosity) of the galaxy, and is unnoticeable for the G1 and G2.

$$\gamma_I = -0.20(16.9 + M_I + 5 \log h_{80}), \quad (8)$$

with  $M_B$  and  $M_I$  being the magnitudes corrected to face-on for the B-band and I-band respectively, and  $H_0 = h_{80} 80 \text{ km/s/Mpc}$ . The conclusions of G95 were the same as those of T98, with a fit described by equation 6, and a luminosity dependence given by

$$\gamma_I = -0.16(15.25 + M_I). \quad (9)$$

However, M03 concluded that a simple linear law as defined in equation 6 was not adequate for describing the dependence of attenuation on inclination observed in their sample. Thus, M03 adopted a bilinear law fitting separately high and low inclination systems as separated by  $\log(a/b) = 0.5$ . Looking for even less linear shapes that better fit their observed colour dependence on inclination, M03 also tried quadratic fits of the form

$$A_{\lambda\nu} = B_{\lambda\nu} + C_{\lambda\nu} \log(a/b) + D_{\lambda\nu} [\log(a/b)]^2, \quad (10)$$

where  $C_{\lambda\nu}$ ,  $B_{\lambda\nu}$ , and  $D_{\lambda\nu}$  are constants that best fit their observed  $\lambda - \nu$  colour dependence on axial ratio.

## 4.2 Comparison of Results with Observations

First, the relative attenuation between the K-band and some other band was examined. As mentioned in the last sub-section, T98 assumed that the extinction effects on the K-band, although small, were not entirely negligible. They assumed that, independent of inclination,  $A_K/A_B$  relative to face-on was 0.15, and  $A_K/A_I$  was

**Table 3.** Ratios of Relative to Face-on Attenuations.

$\theta$ (deg)	$A_K/A_I$		$A_K/A_B$	
	X99	Z94	X99	Z94
0	0	0	0	0
35.4	0.30	0.42	0.09	0.20
50.7	0.30	0.40	0.14	0.21
63.2	0.39	0.35	0.21	0.20
74.4	0.34	0.35	0.20	0.23
85	0.38	0.39	0.26	0.28
90	0.41	0.43	0.30	0.32
Average	0.39	0.33	0.20	0.24

The ratios of relative to face-on attenuations between the K, I and B bands for the Xilouris and Zaritsky gradients at different inclinations for the Sbc galaxy model.

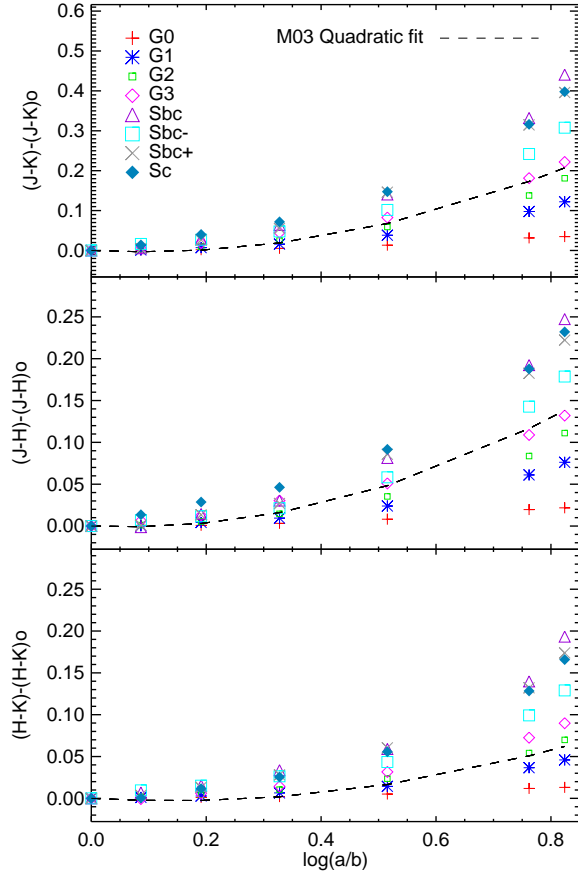
0.25. Our results for these ratios with both the X99 and Z95 gradients are given in Table 3.

Table 3 shows that the average relative attenuations found in our simulations when the Xilouris gradient is assumed (0.20 and 0.39 for  $A_K/A_B$  and  $A_K/A_I$  respectively) are just a little higher than the ratios assumed by T99. However, these ratios vary significantly and in a non-trivial manner with inclination. This was not considered by T98. If this fact is taken into account, their values of observed attenuations should be about 15% higher for large edge-on galaxies. For smaller galaxies and intermediate inclinations the difference is not as large.

Figure 3 shows a direct comparison of the attenuation dependence on inclination and on luminosity with observations. For the luminous galaxies, the Sbc variants, the Sc, and the G3, the Xilouris gradient results in edge-on attenuations which are roughly consistent with the observations. However, this gradient is too steep for the low-luminosity galaxies, producing too little attenuation compared to observations, and X99 only studied large spirals. For this reason, the metallicity gradient for the G2, G1 and G0 galaxies was taken from the results of MA04. In some cases, notably the G3, G2 and G1, the no-gradient simulations seem to match the observations best, but as galaxies are observed to have metallicity gradients, this model is not acceptable and we chose the simple alternative of using the X99 gradient for the luminous galaxies and the MA04 gradient for the smaller ones.

It is apparent from Figure 3 that, although the simulations match some of the observed amplitudes, the dependence of attenuation on inclination is certainly not linear; a relation of the form  $A_\lambda = \gamma_\lambda \log(a/b)$  is not appropriate. The bilinear law adopted by M03 (dashed green in Figure 3) suggests a less linear relation, but still is not similar to what we obtain in the simulations. We also compared the M03 quadratic fits with our simulations. M03 (see Figure 4 in M03) used the statistical average of the colour dependence on inclination observed in their full sample to obtain the fits shown in Figure 4. In order to compare with them, we observed the colour dependence on inclination for each of our eight simulated galaxies, using the adopted gradients for each (see Table 2); this is shown in Figure 4. The shape of the quadratic fits agrees rather well with the results of the simulations.

Lastly, we compared the attenuation dependence on luminosity in our galaxy models with what was observed by G95 and T98. T98 gives results of luminosity dependence for both the I and B bands (equations 7 and 8), while G95 only gives results for the I-band (equation 9). This is shown in Figure 5, which illustrates that



**Figure 4.** The colours J-K, J-H, and H-K relative to face-on plotted against the log of the axial ratio. The black dashed lines represent the quadratic fits described by equation 10. Over-plotted are the colour dependencies found in our models. We do not make a best fit to our points due to the fact that we have more bright galaxies than faint galaxies. The shape between simulations and observations is very similar, and a relation of the form given by equation 10 accurately describes the attenuation dependence on inclination in our simulations.

our points closely follow the fits of G95 and T98, supporting the conclusion that the adopted metallicity gradients are good for our galaxy models. These gradients and the face-on luminosities of our galaxy models when using these gradients are given in Tables 2 and 4.

So far we have been examining the attenuation in certain filter bands. However, SUNRISE calculates dust attenuation at all wavelengths, so we can also calculate the total bolometric stellar luminosity that is absorbed by dust and consequently re-emitted in the infrared. When mid/far-IR observations are available, this “bolometric attenuation” provides a sensitive measure of the total amount of dust, thus avoiding the problem of determining the face-on attenuation.

In order to compare with the Spitzer Infrared Nearby Galaxies Survey (SINGS) sample (Dale et al. 2007, hereafter D07), we have calculated the infrared-to-ultraviolet ratios in our models in the same manner as they did, by dividing the total infrared luminosity (TIR) with the ultraviolet luminosity given by the sum of the luminosities at 1500 Å and 2300 Å (i.e. the FUV and NUV filter bands of the GALEX satellite). Figure 6 shows the results for our

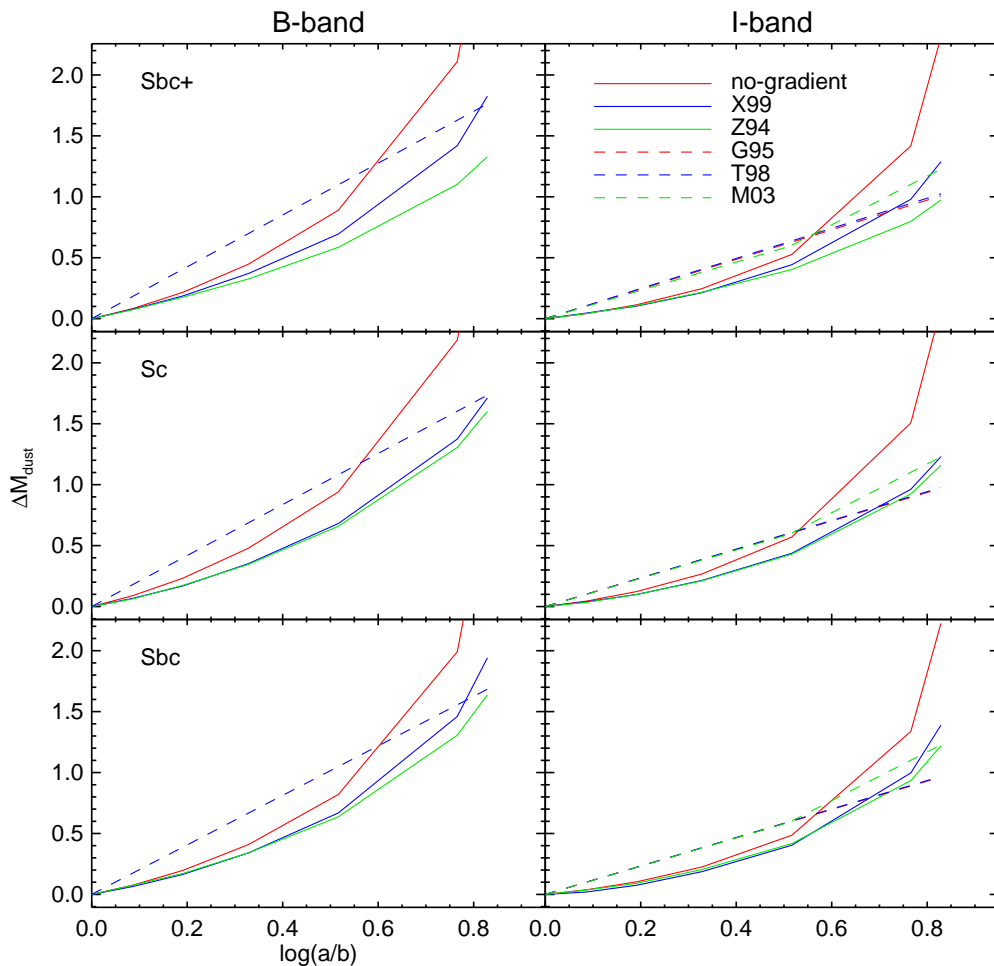


**Figure 3.** Plots of attenuation relative to face-on vs. the log of the axial ratio, in the B-band (left column) and the I-band (right column), for our three most luminous galaxy models: the Sbc+, Sc, and Sbc (top to bottom). The solid lines represent the simulations for two metallicity gradients, Z94 (green) and X99 (blue), and a run with no gradient (red). Dashed lines are the best fits to the observations of G95, T98 and M03. The green dashed line is the bilinear line adopted by M03, valid only for their most luminous galaxies, while the rest are given by equations 7, 8 and 9 varying with luminosity. Although it is not evident if one of the gradients matches better the amplitude of the observations in I-band, it is noticeable that the X99 gradient matches the edge-on attenuations better than the Z94 gradient in the B-band (especially considering that T98 observations should be about 15% higher due to K-band attenuation), hence we adopt it as our preferred gradient for the most luminous galaxy models. Our simulations evidently do not match the shape of the fits adopted by observers, as they predict less attenuation for intermediate inclinations than the observations show.

**Table 4.** Luminosities

Galaxy	$M_B$	$M_I$	$M_K$	$L_{abs}/L_{bol}$
Sbc+	-21.6	-22.9	-23.2	0.48
Sbc	-21.4	-22.5	-22.8	0.44
Sc	-21.2	-22.6	-22.6	0.46
Sbc-	-20.3	-21.6	-21.9	0.37
G3	-20.4	-22.0	-22.4	0.32
G2	-19.2	-20.8	-21.2	0.32
G1	-17.9	-19.6	-19.9	0.14
G0	-16.0	-17.6	-18.1	0.02

Face-on luminosities in B, I, and K bands for our set of galaxy models when the adopted metallicity gradients of Table 2 are used. The last column shows the fraction of bolometric luminosity which is absorbed by dust.

different models at different inclinations. We only compare within the range of inclinations included in the D07 sample (i.e. 0 to 70

degrees). Comparing the range of infrared-to-ultraviolet ratios for the Sbc, G3 (which approximates an Sb type), and Sc models with the galaxies of these types observed by D07 (see Figure 5 in D07), the simulated galaxies show slightly lower attenuation. While D07 observed ratios from about 1 to 10, we obtain ratios from about 1.5 to 7, but the SINGS sample only contains a few star-forming galaxies with these morphological types. Overall, the amount of dust attenuation in our galaxies, as given by the infrared-to-ultraviolet flux ratio, appears to be fairly close to what is observed in real galaxies.

Another measurement of the bolometric attenuation was done by Popescu & Tuffs (2002) using the ISOPHOT instrument on the ISO satellite, who found correlations between the overall attenuation and the Hubble type of a sample of galaxies in the Virgo cluster. They obtained a mean bolometric attenuation in galaxies of type Sab-Sc of about 0.23. Comparing the values in Table 4 for the G3, Sbc-, Sbc, Sbc+, and Sc to the results of Popescu & Tuffs (2002), the simulations have attenuations that are about 15 – 20% higher. (The simulated galaxies here have slightly lower bolometric attenu-

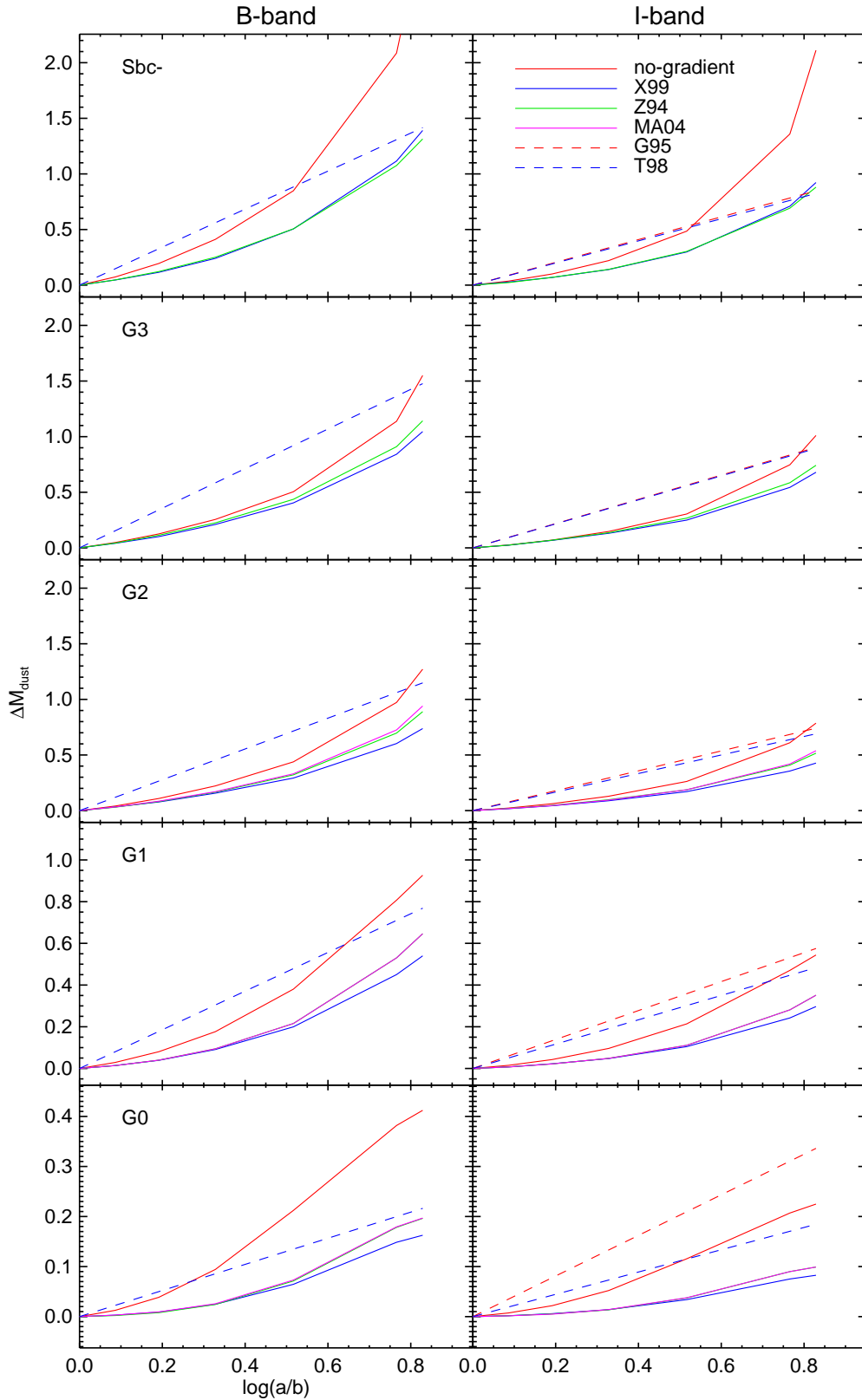


**Figure 3** – *continued* The Sbc-, G3, G2, G1, and G0 (top to bottom). We can see how, for the G-series, the relative attenuation with the X99 (solid blue) gradient falls below the observations. Of the observed metallicity gradients, those of MA04 (solid pink) give a relative attenuation that is closest to what is observed, hence we have adopted these as our preferred gradients for the G0, G1, and G2. The results using the Z94 (solid green) for the G0, G1, and G2 are similar and overlap in some cases with those of MA04. For the lower-mass galaxies, using constant metallicity is sometimes the best-fitting model. Nevertheless, the no-gradient model was not adopted since no observations support such a metallicity distribution.



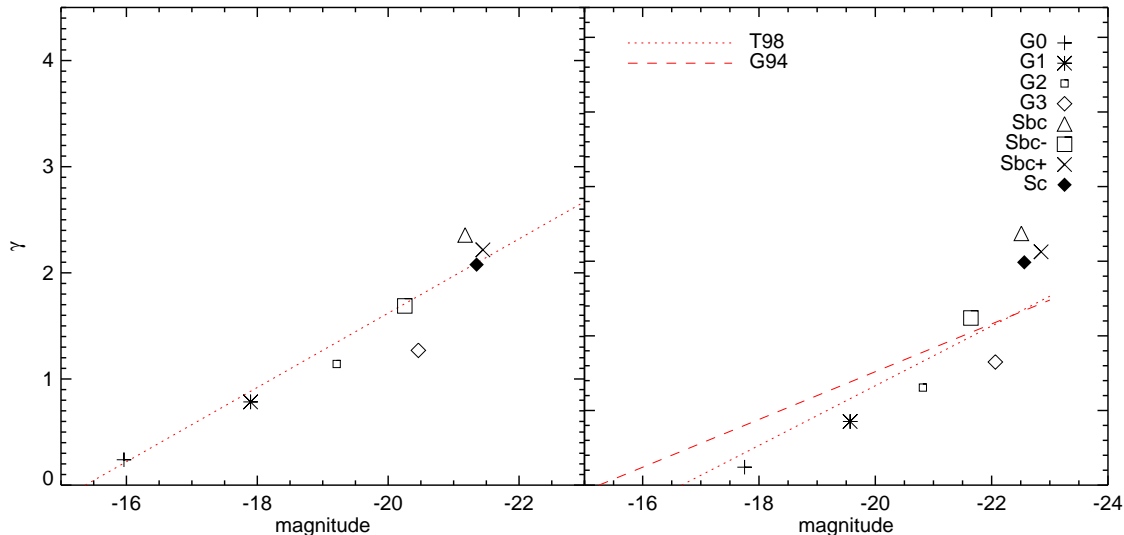


**Figure 5.** The attenuation parameter  $\gamma$ , as defined by the relation 6, plotted against the face-on magnitudes of all our models in the B-band (left), and the I-band (right). The dotted and dashed lines are the best fits to the observations of T98 and G95 respectively. Our points match the I-band observations less well, but the agreement is still reasonable given the fact that we only have two galaxies fainter than  $-20$ .

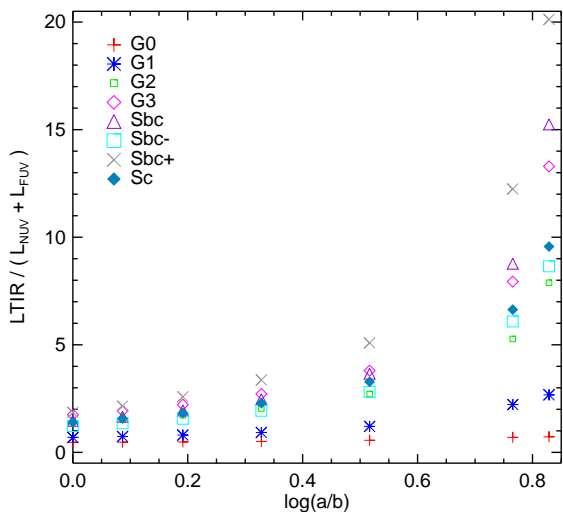


**Figure 6.** Infrared-to-ultraviolet ratios for our models, as a function of inclination. This figure can be directly compared to Figures 4 & 5 in D07. Compared to the SINGS galaxies of the corresponding morphological types, the simulations show slightly lower dust attenuations but cover roughly the same range of values. The total infrared emission in our models thus appears to be consistent with what is observed by SINGS.

ations than those previously obtained by Jonsson et al. (2006) using simulations with constant metallicity.)

Apparently, the results of D07 and Popescu & Tuffs (2002) are mutually inconsistent. It is possible that the ISOPHOT observations, only sensitive to wavelengths longer than  $60 \mu\text{m}$ , missed a significant fraction of the dust luminosity at shorter wavelengths. Another possibility is that the spiral galaxies in the Virgo cluster have systematically lower gas content and lower star-formation rates than the average field spiral. Overall, the fact that our galaxies

have slightly lower bolometric attenuation compared to the newer and higher-quality data of the SINGS galaxies, as well as slightly lower values of  $A_\lambda$ , especially at intermediate inclinations, paints a consistent picture that the simulations have dust attenuations on the slightly low side of observed galaxies of the same morphological types.

## 5 COMPARISON WITH OTHER MODELS

A simple way to model dust attenuation in the disk of galaxies is to perform radiative transfer calculations in smooth exponential distributions of stars and dust, disregarding scattering. This is unrealistic but helps to understand the behaviour of attenuation when changing parameters such as inclination or dust-to-stellar scalelengths/scaleheights. Disney et al. (1989) developed a triple exponential model in which a single scalelength describes the radial distribution of stars and dust, and two vertical scaleheights, one for dust and one for stars, describe the vertical distributions of the model. This same model was later used and extended by Giovanelli et al. (1994) and M03. Motivated by the results of X99, we explored the same model but allowing different scalelengths for dust and stars (a “quadruple exponential” model). In a model like this, the emissivity and absorption coefficients of the radiative-transfer equation would be given by

$$\epsilon(r, z) = \epsilon_o \exp\left(-\frac{r}{R_s} - \frac{|z|}{Z_s}\right) \quad \text{and} \quad (11)$$

$$\kappa(r, z) = \kappa_o \exp\left(-\frac{r}{R_d} - \frac{|z|}{Z_d}\right), \quad (12)$$

with  $\epsilon_o$  and  $\kappa_o$  being the emissivity and the absorption coefficient at the centre, respectively,  $R_s$  and  $Z_s$  the scalelength and scaleheight of the stars, respectively, and  $R_d$  and  $Z_d$  the scalelength and scaleheight of the dust, respectively. Figure 7 plots the resulting attenuation dependence on inclination for different values of  $\lambda = R_d/R_s$ , and with  $\xi = Z_d/Z_s = 0.5$ ,  $q = Z_s/R_s = 0.15$ , and  $\tau = 1$ ,

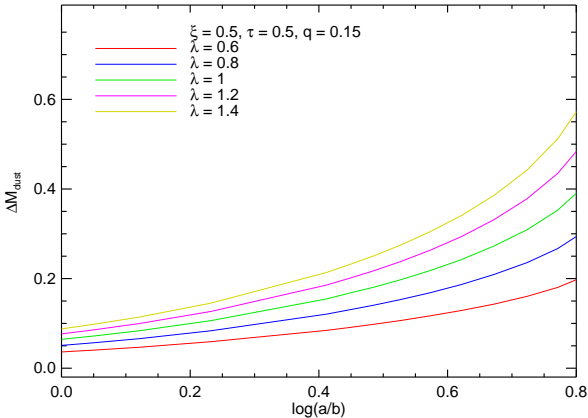


**Figure 7.** Attenuation relative to face-on vs. the  $\log$  of the axial ratio for the “quadruple exponential” model when different values of  $\lambda = R_d/R_s$  are given. We can see that the different values of  $\lambda$  result in different magnitudes of edge-on attenuations, but do not affect the quadratic shape of the relation much.

where  $\tau$  is the central face-on optical depth

$$\tau = \int \kappa(0, z) dz = 2\kappa_o \int_0^\infty \exp\left(-\frac{z}{Z_d}\right) dz = 2\kappa_o Z_d. \quad (13)$$

Disney et al. (1989), Giovanelli et al. (1994), and M03 show how this simple model behaves when different values of  $\xi$ ,  $q$ , and  $\tau$  are given. We find that when different values of  $\lambda$  are assumed the edge-on attenuation varies significantly, but the shape of the curve remains the same (see Figure 7).

More sophisticated radiative transfer models where anisotropic scattering is considered and different parameterisations and spatial distributions of clumps are included can be found extensively in the literature (see the introductions of Pierini et al. (2004) and Tuffs et al. (2004) for nice reviews of the history of these models), but few explore the consequences of structure such as spiral arms in the resulting attenuations (Corradi et al. 1996; Semionov et al. 2007). If we compare our results for the attenuation dependence on inclination (Figure 3) with some of these models, i.e. Giovanelli et al. (1994); Bianchi et al. (1996, 2000); Ferrara et al. (1999); Baes & Dejonghe (2001); Byun et al. (1994); Tuffs et al. (2004) we cannot see any significant difference that can be attributable to the geometry of our simulated galaxies.

The dependence of attenuation on wavelength in our Sbc model (which has a central optical depth  $\tau$  close to 2) has been compared with that of Pierini et al. (2004, hereafter P04), when we adopt their model (see Table 1 of P04). The results are plotted in Figure 8. We did not find any significant differences between the attenuation curves in P04 and ours when using the same dust model, suggesting that the presence of spiral arms or any structure of similar size in our simulations does not affect the attenuation significantly.

It is important to notice that none of the above models, for values of dust-to-star scale length/height ratios and central optical depths normally observed in spiral galaxies, show attenuations that vary linearly as a function of  $\log(a/b)$ . Ferrara et al. (1999) found that only values of dust-to-star scaleheight ratios of about 2.5 resulted in an attenuation dependence on inclination comparable to that observed by de Vaucouleurs et al. (1991), but scaleheight ratios of this magnitude are far from what observations suggest. Thus, the

disagreement regarding the behaviour of the attenuation as a function of inclination is not limited to our models and it is clear that further work is needed to understand this discrepancy.

In the near future, the images that have been generated with SUNRISE for this work will be analysed in order to quantify the changes in the apparent scalelengths, central surface brightness, and axis ratios due to the presence of dust, in a similar manner to what was done by Möllenhoff et al. (2006).

## 6 SUMMARY AND CONCLUSIONS

### 6.1 Summary

Simulations of dust attenuation were performed in eight different SPH simulations of isolated spiral galaxies, assuming different metallicity gradients. The three metallicity gradients explored were  $-0.05$  dex/kpc, as suggested by Z94, the metallicity gradient required to obtain a dust scalelength that is 1.4 times greater than the stellar scalelength, as was observed by X99, and metallicities obtained from the dependence of the metallicity gradient on luminosity observed by MA04. We compared the dependence of attenuation on inclination resulting from these gradients with observations by G95, T98, and M03, finding that our simulations do not follow a linear dependence on  $\log(a/b)$ . The non-linear fits adopted by M03 from their observations of colour dependence on inclination were also compared to the results of the simulations, giving a more satisfactory match to the shape. The preferred gradients adopted from the above comparisons were used to obtain a relation between the relative face-on to edge-on attenuation and luminosity, finding that it followed a rather linear behaviour that closely matches the observations of G95, and T98. Finally, we compare our results to previous models of galactic disks where structure such as spiral arms are disregarded, showing that the curves obtained from our simulations can be explained in terms of the same parameters (no parameters to account for large structure resolved by our simulations are necessary), and that the shape at intermediate inclinations is very similar for both the models and our simulations.

### 6.2 Conclusions

1. When the radial metallicity gradient implied by the results of X99 is assumed, the observed amplitudes of relative attenuation from face-on to edge-on in our most luminous galaxies agree fairly well with the results of the simulations. The fainter galaxies of the set required less steep gradients, and we adopted the gradients from MA04 for the G0, G1, and G2. This is not surprising considering that the X99 results were obtained only for big spiral galaxies, and may not be valid for smaller spiral galaxies.

2. Results for the ratios of attenuations between different bands in Table 3 show that there is always some attenuation in the near infrared (K-band), with an inclination dependence such that the attenuation in the K-band certainly is significant at high inclinations. Our results show that the relative to face-on attenuation in the K-band can be as high as 30% of the attenuation in the B-band when the Sbc model is seen edge-on, enough to introduce bias of about 15% if this is neglected.

3. Reproducing observed edge-on attenuations and their dependence on luminosity does not imply that the simulations correctly describe the extinction effects across all inclinations. The disagreement in the shape of the attenuation vs. inclination relations between observations and simulations suggests that either a simple

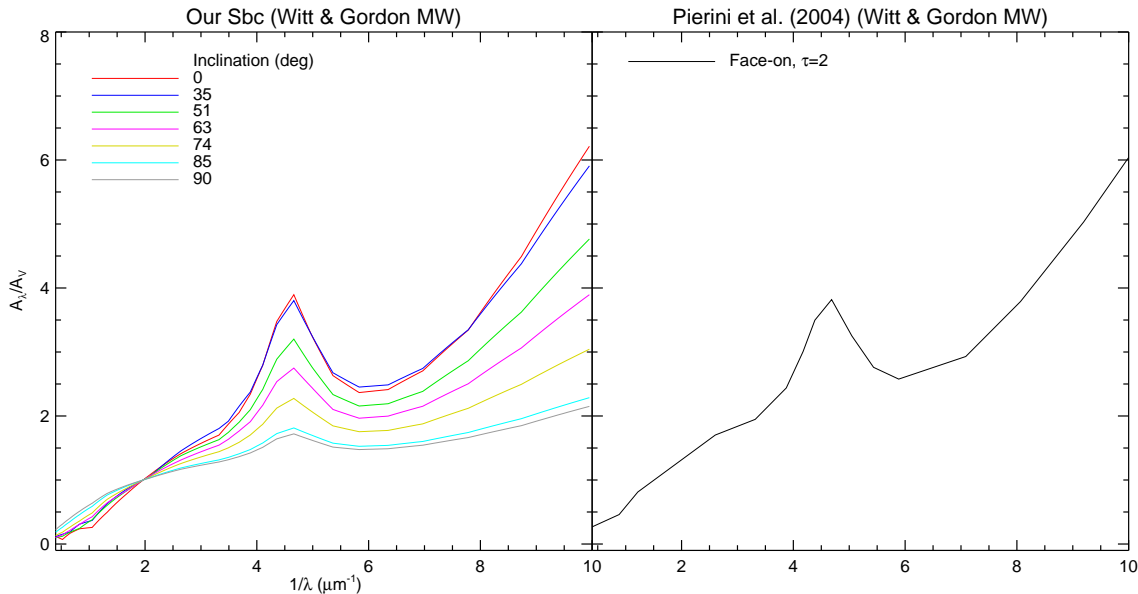


**Figure 8.** Normalised attenuation curves for our Sbc model when the dust model adopted by Pierini et al. (2004) is used in our simulation (left), and for the P04 homogeneous face-on model with  $\tau = 2$  (right). We can see that there are no significant differences that can be related to the structure resolved in our hydrodynamic simulations. Figure 18 of P04 shows the dependence of their model with inclination, but only for  $\tau = 1$ , thus we have not plotted these results here.

linear extinction law of the form  $A_\lambda = \gamma_\lambda \log(a/b)$  is only a rough approximation to real galaxies, or that our simulations are not good models of observed galaxies. It is difficult to know whether the linear relations given by G95 and T98 are the result of uncertainty in the observations, or if the relations obtained in the simulations really are excluded by the data. The most recent study by M03, which also has the largest sample, suggests that a linear extinction law is not appropriate, and they propose both a bilinear law and a quadratic law. The quadratic fits obtained by M03 have the same shape at intermediate inclinations as our simulations. We have too few simulated galaxies to perform an adequate statistical fit as has been done by M03, hence we cannot adequately compare with the amplitude given by these quadratic fits. However, we note that a good way to describe the attenuation dependence on inclination found in the set of simulations performed here is by a quadratic law of the form

$$\Delta M = B + C \log(a/b) + D [\log(a/b)]^2, \quad (14)$$

as proposed by Masters et al. (2003). Other models obtain a shape similar to ours, so this disagreement is not unique to our simulations

4. The bolometric attenuations in our simulations as measured by the infrared-to-ultraviolet flux ratio are consistent with, but possibly on the low side of, the range observed for galaxies of corresponding morphological type in the SINGS sample by D07. However, the bolometric attenuations in the simulations are significantly larger than those obtained in an older study by Popescu & Tuffis (2002). This indicates that the two observational studies are in conflict, regardless of the uncertainty of the simulated results, as it will be difficult to match both results simultaneously.

5. The attenuation vs. inclination relation obtained from models that do not take account of spiral structure is very similar in shape (a quadratic relation) to our calculations using hydrodynamic galaxy models, and there is no evidence to conclude that the inclusion of complex geometries like spiral arms makes a difference

in the attenuation as a function of inclination nor wavelength. Of course, this is not true for highly disturbed systems like merging galaxies.

This work was supported by programs HST-AR-10678 and HST-AR-10958, provided by NASA through grants from the Space Telescope Science Institute, which is operated by the Association of Universities for Research in Astronomy, Incorporated, under NASA contract NAS5-26555.

This research used computational resources of the National Energy Research Scientific Computing Center (NERSC), which is supported by the Office of Science of the U.S. Department of Energy, and of the NASA Advanced Supercomputing Division (NAS).

## REFERENCES

- Baes M., Dejonghe H., 2001, *MNRAS*, 326, 733
- Bell E. F., de Jong R. S., 2000, *MNRAS*, 312, 497
- Bertschinger E., Dekel A., Faber S. M., Dressler A., Burstein D., 1990, *ApJ*, 364, 370
- Bianchi S., Ferrara A., Davies J. I., Alton P. B., 2000, *MNRAS*, 311, 601
- Bianchi S., Ferrara A., Giovanardi C., 1996, *ApJ*, 465, 127
- Bosma A., Byun Y., Freeman K. C., Athanassoula E., 1992, *ApJ*, 400, L21
- Burstein D., Haynes M. P., Faber M., 1991, *Nature*, 353, 515
- Byun Y. I., Freeman K. C., Kylafis N. D., 1994, *ApJ*, 432, 114
- Corradi R. L. M., Beckman J. E., Simonneau E., 1996, *MNRAS*, 282, 1005
- Cowie L. L., Songaila A., 1986, *ARA&A*, 24, 499
- Cox T. J., 2004, PhD thesis, University of California, Santa Cruz, <http://physics.ucsc.edu/~tj/work/thesis>
- Cox T. J., Jonsson P., Primack J. R., Somerville R. S., 2006, *MNRAS*, 373, 1013

- Cox T. J., Jonsson P., Somerville R. S., Primack J. R., Dekel A., 2007, MNRAS, submitted (arXiv:0709.3511v1)
- Dalcanton J. J., Yoachim P., Bernstein R. A., 2004, ApJ, 608, 189
- Dale D. A., Gil de Paz A., Gordon K. D., Hanson H. M., Armus L., Bendo G. J., Bianchi L., Block M., Boissier S., Boselli A., Buckalew B. A., Buat V., Burgarella D., Calzetti D., Cannon J. M., Engelbracht C. W., Helou G., Hollenbach D. J., 2007, ApJ, 655, 863
- de Jong R. S., 1996, A&A, 313, 45
- de Vaucouleurs G., 1948, Annales d'Astrophysique, 11, 247
- de Vaucouleurs G., de Vaucouleurs A., Corwin Jr. H. G., Buta R. J., Paturel G., Fouque P., 1991, S&T, 82, 621
- Dekel A., Eldar A., Kolatt T., Yahil A., Willick J. A., Faber S. M., Courteau S., Burstein D., 1999, ApJ, 522, 1
- Disney M., Burstein D., Haynes M. P., Faber S. M., 1992, Nature, 356, 114
- Disney M., Davies J., Phillipps S., 1989, MNRAS, 239, 939
- Dwek E., 1998, ApJ, 501, 643
- Ferrara A., Bianchi S., Cimatti A., Giovanardi C., 1999, ApJS, 123, 437
- Freedman W. L., Madore B. F., Gibson B. K., Ferrarese L., Kelson D. D., Sakai S., Mould J. R., Kennicutt Jr. R. C., Ford H. C., Graham J. A., Huchra J. P., Hughes S. M. G., Illingworth G. D., Macri L. M., Stetson P. B., 2001, ApJ, 553, 47
- Giovanelli R., Haynes M. P., Salzer J. J., Wegner G., da Costa L. N., Freudling W., 1994, AJ, 107, 2036
- Giovanelli R., Haynes M. P., Salzer J. J., Wegner G., da Costa L. N., Freudling W., 1995, AJ, 110, 1059 (G95)
- Holwerda B. W., González R. A., van der Kruit P. C., Allen R. J., 2005, A&A, 444, 109
- Jarrett T. H., Chester T., Cutri R., Schneider S. E., Huchra J. P., 2003, AJ, 125, 525
- Jarrett T. H., Van Dyk S., Chester T. J., 2001, in 198th AAS Meeting Vol. 33 of Bulletin of the American Astronomical Society, 2MASS Large Galaxy Atlas. American Astronomical Society, pp 856–
- Jonsson P., 2006, MNRAS, 372, 2
- Jonsson P., Cox T. J., Primack J. R., Somerville R. S., 2006, ApJ, 637, 255
- Kennicutt R. C., 1998, ApJ, 498, 541
- Kuchinski L. E., Terndrup D. M., Gordon K. D., Witt A. N., 1998, AJ, 115, 1438
- Kylafis N. D., Bahcall J. N., 1987, ApJ, 317, 637
- Kylafis N. D., Misiriotis A., Papamastorakis J., Xilouris E. M., 2001, Ap&SS, 276, 531
- Leitherer C., Schaerer D., Goldader J. D., Delgado R. M. G., Robert C., Kune D. F., de Mello D. F., Devost D., Heckman T. M., 1999, ApJS, 123, 3
- MacArthur L. A., Courteau S., Bell E., Holtzman J. A., 2004, ApJS, 152, 175 (MA04)
- Masters K. L., Giovanelli R., Haynes M. P., 2003, AJ, 126, 158 (M03)
- Matthews L. D., Wood K., 2001, ApJ, 548, 150
- Möllenhoff C., Popescu C. C., Tuffs R. J., 2006, A&A, 456, 941
- Moriondo G., Giovanelli R., Haynes M. P., 1998, A&A, 338, 795
- Pierini D., Gordon K. D., Witt A. N., Madsen G. J., 2004, ApJ, 617, 1022
- Popescu C. C., Tuffs R. J., 2002, MNRAS, 335, L41
- Schmidt M., 1959, ApJ, 129, 243
- Semionov D., Kodaira K., Stonkute R., Vansėvicius V., 2007, Baltic Astronomy, 15, 581
- Silva L., Granato G. L., Bressan A., Danese L., 1998, ApJ, 509, 103
- Springel V., Hernquist L., 2002, MNRAS, 333, 649
- Springel V., Yoshida N., White S. D. M., 2001, New Astronomy, 6, 79
- Tuffs R. J., Popescu C. C., Völk H. J., Kylafis N. D., Dopita M. A., 2004, A&A, 419, 821
- Tully R. B., Pierce M. J., Huang J., Saunders W., Verheijen M. A. W., Witchalls P. L., 1998, AJ, 115, 2264 (T98)
- Valentijn E. A., 1994, MNRAS, 266, 614
- van der Kruit P. C., Searle L., 1981, A&A, 95, 105
- Weingartner J. C., Draine B. T., 2001, ApJ, 548, 296
- Xilouris E. M., Byun Y. I., Kylafis N. D., Paleologou E. V., Papamastorakis J., 1999, A&A, 344, 868 (X99)
- Zaritsky D., Kennicutt R. C., Huchra J. P., 1994, ApJ, 420, 87 (Z94)